Rare Metal Materials and Engineering
Volume 49, Issue 5, May 2020
Available online at www.rmme.ac.cn

Science Press

Cite this article as: Rare Metal Materials and Engineering, 2020, 49(5): 1576-1582.

ARTICLE

Pore Characteristics and Mechanical Behavior of Spark Plasma Sintered Porous Zn-Mg Alloy for Biomedical Applications

Cui Zeqin[1,2,3], **Li Weijian**[1,2,3], **Ma Lili**[1], **Yang Ruihong**[1], **Gong Dianqing**[1,2,3]

[1] Taiyuan University of Technology, Taiyuan 030024, China; [2]Shanxi Key Laboratory of Advanced Magnesium-based Materials, Taiyuan 030024, China; [3] Key Laboratory of Interface Science and Engineering in Advanced Materials, Ministry of Education, Taiyuan 030024, China

Abstract: Porous Zn-*x*Mg alloy scaffolds (*x*=5 wt%, 10 wt%, 15 wt%) were fabricated as bone tissue engineering scaffold by spark plasma sintering (SPS) using the same volume content space holder (NaCl). The effect of Mg content on the mechanical properties and microstructural characterizations of the porous Zn-*x*Mg alloys scaffold was revealed. Results show that with the increasing content of Mg from 5 wt% to 15 wt%, the porosity increases from 40.3% to 54.3% and the mean open pore size increases from 289 μm to 384 μm due to the dealloying effect of Mg. Mechanical test results indicate that porous Zn-Mg alloy is a typical elastic-brittle metallic foam and porous Zn-10Mg is the best among three scaffolds. The strength and elastic module of the scaffolds show good biomechanical compatibility and is promising to be used as a lower load-bearing implant material.

Key words: porous zinc-based alloy; spark plasma sintering (SPS); porous structure; mechanical properties

Nowadays, biomedical porous metal materials as a new type structure and functional materials are followed with interest. Porous structure can not only provide large inner space for ingrowth of new bone tissue and capillaries, but also contribute to reduction of stress-shielding effect due to its low elastic modulus[1-3]. A variety of biomaterials have been developed and designed into porous structures, including degradable metals. The degradation rate of zinc, as one of biodegradable and non-toxic elements, is relatively lower than that of magnesium. According to the standard electrode potential Mg(-2.37 V)< Zn(-0.763 V)< Fe(-0.44 V), the degradation rate of zinc falls in between the rates of Mg and Fe[4]. Zinc is also one of necessary nutrient element for human, and it plays an important role in the metabolism of human body, such as involving in the synthesis of more than 80 kinds of enzymes, and directly participating in cell division and regeneration[5]. However, the use of pure Zn in porous scaffold is rather limited because of its insufficient mechanical properties, especially the strength[6,7]. Therefore, modifying the mechanical properties by adding alloying elements would be an effective way. Currently, Zn-Cu, Zn-Sr, Zn-Ag, Zn-Mg alloys were developed as biodegradable materials[8-11]. Among these zinc-based alloys, both Zn and Mg as biodegradable and necessary elements for human have received great attention. Therefore, in this work, Mg was chosen as the alloying element to form porous Zn-Mg binary alloys scaffold.

Usually, the main methods for fabricating porous metal scaffolds include, air pressure infiltration method (APIM)[6,10,11], additive manufacturing (AM) [12,13] and powder metallurgy (PM) [1-3,14,15]. Compared with the APIM and AM, the PM is more convenient and cheaper. In this method, carbamide, NaCl and ammonium bicarbonate particles were usually used as space holders in the PM and APIM. Among the three space holders, NaCl particle has good solubility and relatively higher melting point (801 °C) than matrix metals, which promises NaCl could not react with matrix metal during sintering.

In this work, porous Zn-*x*Mg alloy scaffolds (*x*= 5, 10, 15, wt%) with space holder were fabricated by spark plasma sin-

---

Received date: May 15, 2019
Foundation item: National Natural Science Foundation of China (51305292); Shanxi Province Natural Science Foundation of China (201801D221089)
Corresponding author: Cui Zeqin, Ph. D., Associate Professor, College of Materials Science and Engineering, Taiyuan University of Technology, Taiyuan 030024, P. R. China, E-mail: cuizeqin@tyut.edu.cn

tering (SPS). In order to make the pores as connected as possible, identical 50% volume content of space holder (NaCl particle) was added in the three components. The effect of Mg addition on the pore characteristics and mechanical properties of porous Zn-Mg alloy scaffolds were investigated in detail. Additionally, the deformation behavior of the porous Zn-Mg alloys scaffolds were analyzed by describing the compressive stress-strain curve and observing the fracture morphology of bending test.

1 Experiment

Commercially pure Zn (99.99%, particle size <50 μm) and pure Mg (99.88%, particle size <50 μm) were used as raw materials. NaCl particles with hexahedron shape (sieved by standard sieves into 100~400 μm) were used as the space holder. Fig. 1a shows the morphology of NaCl particles.

Power Zn and Mg were milled in an agate pot at a speed of 350 r/min for 4 h by planetary ball milling (QM-QX 0.4L). The mass ratio of the power to agate ball was 2:1. Fig. 1b shows the Zn-Mg particles after ball milling, whose average size is 5~25 μm. After that, the sieved NaCl particles were mixed into the Zn-Mg powders. No agate ball or lubricant was added during the second mixing. In order to avoid oxidation, the entire ball milling process was carried out under argon protection. Then these mixtures were fed into ϕ30 mm cylindrical-shaped graphite die. Spark plasma sintering (SPS-331LX Fuji Electronic Industrial Co., Ltd, Japan) process consisted of three steps: heating up to 575 K at the rate of 75 K·min^{-1}, then heating up to 635 K at the rate of 30 K·min^{-1} and keeping at 635 K for 5 min. The entire sintering process was under axial applied stress of 5 MPa in vacuum. After cooling to room temperature, the obtained specimens were subjected to ultrasonic treatment in deionized water to remove the space holder.

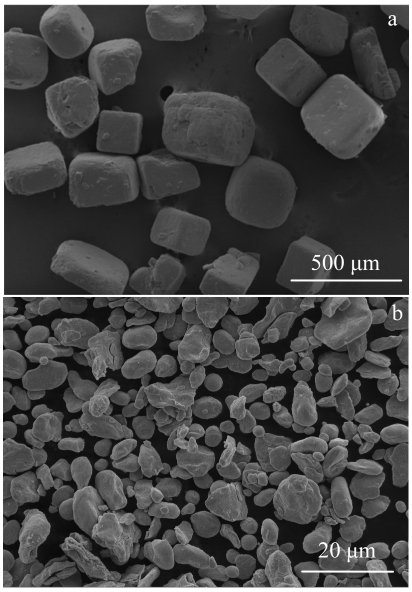

Fig.1 SEM images of raw materials: (a) space holder NaCl particles sieved in the range 100~400 μm, (b) Zn and Mg mixed powder after 4 h ball-milling

The phase constitutes were detected by X-ray diffraction (XRD, Rigaku D/Max 2550V) using Cu Kα radiation at a scanning rate of 4°·min^{-1}. The pore structure was observed by using optical microscopy (OM, Leica DM2700M) and scanning electron microscopy (SEM, Mira3) equipped with an energy dispersive spectroscopy (EDS, OXford). The average size of open pore was analyzed by the Image Pro Plus 6.0 using OM images. The total porosity (P) of the porous Zn-Mg alloys was calculated by using the Mass-Volume principle:

$$P = \left(1 - \frac{M}{V \cdot \rho_s}\right) \times 100\% \tag{1}$$

Where, M and V are the mass and volume of the porous samples, respectively. And ρ_s is the theoretical density of Zn-xMg/NaCl composite.

The specimens for compressive tests were machined into cylinders having the size of ϕ 6 mm×11 mm, and the sample size for three-point bending tests was 25 mm × 6 mm × 6 mm. Uniaxial compression was loaded with the speed of 0.5 mm/min using DNS100 testing machine, at room temperature of 25 °C. Three samples were tested for each component. The fracture surfaces following three-point bending tests were observed by SEM.

2 Results and Discussion

2.1 Pore structure characterization

The digital image of porous Zn-xMg (x=5 wt%, 10 wt%, 15 wt%) alloy scaffolds is shown in Fig.2. Optical micrographs at latitudinal cross-section of porous Zn-Mg alloy samples with different contents of Mg are shown in Fig.3. It can be found from Fig.3a that those pores made by removing NaCl particles have regular square shapes. However, it can be seen from Fig. 3b and 3c that with the content of Mg increasing, the independent pores turn into interconnected and the width of interconnected galleries between pores widen obviously, resulting in the open pores size increase.

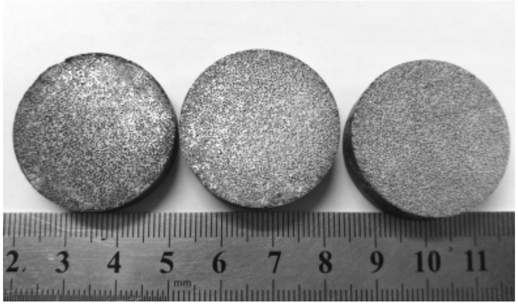

Fig.2 Digital image of porous Zn-xMg alloy scaffolds

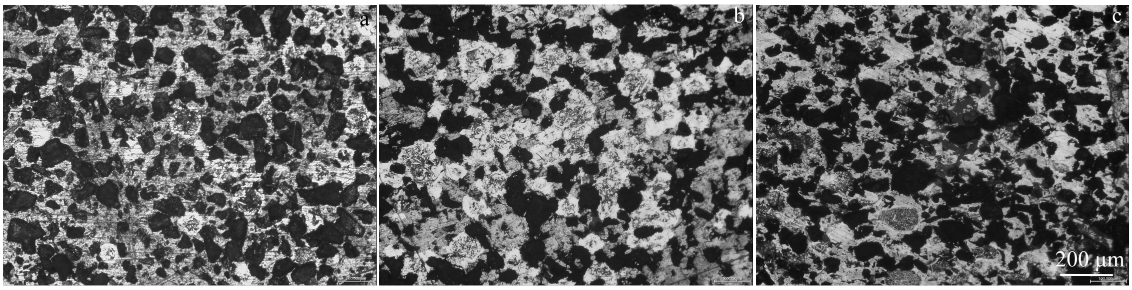

Fig.3 Optical micrographs of porous Zn-Mg scaffolds with different Mg mass contents (black area is the pore): (a) porous Zn-5Mg, (b) porous Zn-10Mg, and (c) porous Zn-15Mg

Fig.4a to 4c show the open pore size statistical distribution of porous Zn-Mg scaffolds. The measured porosity and mean pore size (an equivalent pore diameter) are shown in Fig.4d. It could be found that with the content of Mg increasing, the porosity increases from 40.3% to 54.3% and average pore size also increases from 289 μm to 384 μm. According to the Ref. [3], the porosity in the range of 30%~50% and the optimal pore size of 100~400 μm are suitable for new bone tissue and capillaries ingrowth. Therefore, the pore characteristics of porous Zn-Mg alloy scaffold can well meet those of bone.

The reason is that the density of Mg (1.74 g/cm^3) is far below that of Zn (7.14 g/cm^3); therefore, although the mass ratio of Mg is lower than that of Zn, the volume ratio of Mg in specimen is not low. In the porous specimen with 15 wt% of Mg, the volume ratio of Mg reaches up to 42.97%. After alloying between Zn and Mg during SPS sintering, there may still remain some pure Mg in samples. When removing the space holder by using ultrasonic dissolution, the remained Mg also reacted with H_2O acutely to produce corrosion products $Mg(OH)_2$[2,3,16]. Meanwhile, the process of dissolving NaCl released some chlorides. The chlorides would react with $Mg(OH)_2$ rapidly, breaking the $Mg(OH)_2$ protective layer and accelerating corrosion rate of Mg. These reactions are expressed as follows:

Anodic reaction $Mg \rightarrow Mg^{2+} + 2e^-$ (2)

Cathodic reaction $2H_2O+2e^- \rightarrow H_2+2OH^-$ (3)

Corrosion products $Mg^{2+} + 2OH^- \rightarrow Mg(OH)_2$ (4)

$Mg(OH)_2 + 2Cl^- \rightarrow MgCl_2 + 2OH^-$ (5)

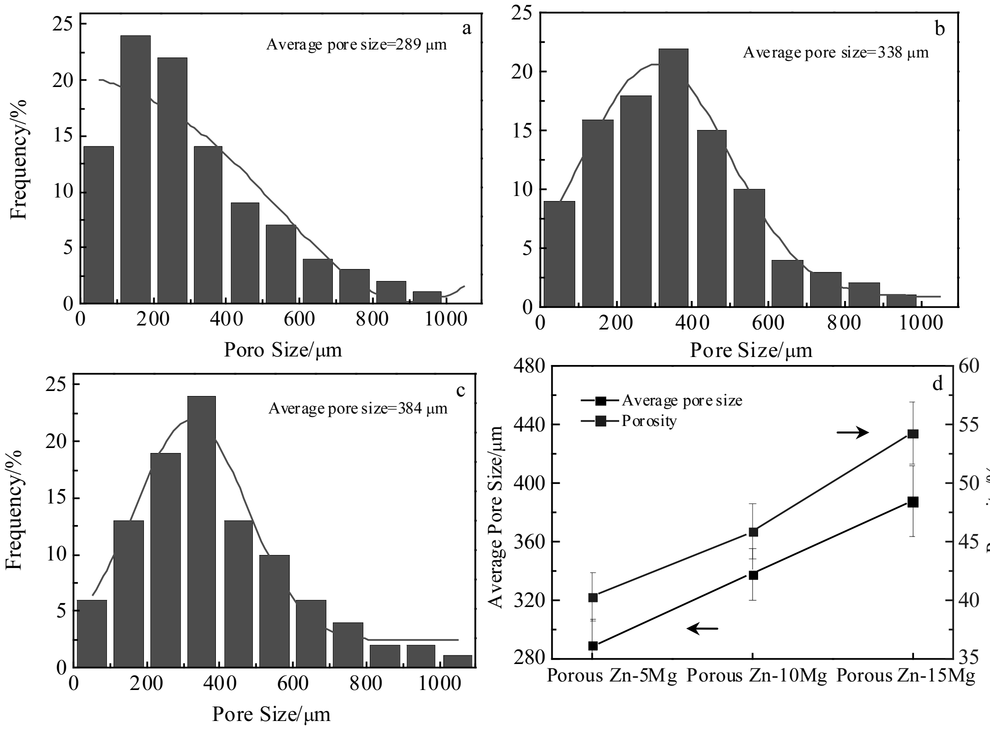

Fig.4 Open pore size statistical distribution of the porous Zn-Mg scaffolds: (a) Zn-5Mg, (b) Zn-10Mg, (c) Zn-15Mg, and (d) porosity and average pore size of porous Zn-Mg alloy scaffolds

Actually, the process of removing space holder (NaCl) is similar to a dealloying process to consume Mg element. The result is that this process makes the pore and pore interconnected. Meanwhile, it also increases the pore size and porosity.

Fig.5 shows the EDS analysis results of the inner pore of porous Zn-10Mg scaffold. Na and Cl were not found in this analyzed region, indicating that the NaCl particles in this range were removed clearly. There was slight oxidation on the inner pore wall, and the mass content of Mg in this region was lower than the initial addition, which confirmed that there has indeed been a slight dealloying process.

Fig.6a to 6c shows the axial cross-sectional photographs of porous Zn-*x*Mg alloy scaffolds. From these figures, it could be found that the inner pores made by removing NaCl particles remained almost equiaxial and distributed evenly, which were not affected by the compression during SPS process. And these images show that the pore walls densified well without macro cracks. Although the porosity of porous Zn-15Mg has reached 54.3%, very close to the volume content of space holder, the porosity of porous Zn-10Mg and porous Zn-5Mg is still lower than 50%. It means that some small size NaCl particles may remain undissolved in closed pores.

2.2 Phase analysis

Fig.7a shows the phase composition of porous Zn-*x*Mg alloys scaffolds. As observed in the XRD patterns, porous Zn-Mg alloys mainly contained two secondary phases $MgZn_2$, Mg_2Zn_{11}, one minor phase ZnO and pure Zn phase. No pure Mg peak was found in Fig.7. Indeed, the elemental Mg of the surface layer of the porous samples has been almost consumed due to the dealloying effect as mentioned above. According to Mg-Zn binary phase diagram, theoretically, the Zn could react with Mg at 625 K[17], causing exsolution precipitation and forming secondary Mg_2Zn_{11}, $MgZn_2$. Fig.7b and Fig.7c are the BSEM image of porous Zn-5Mg and EDS

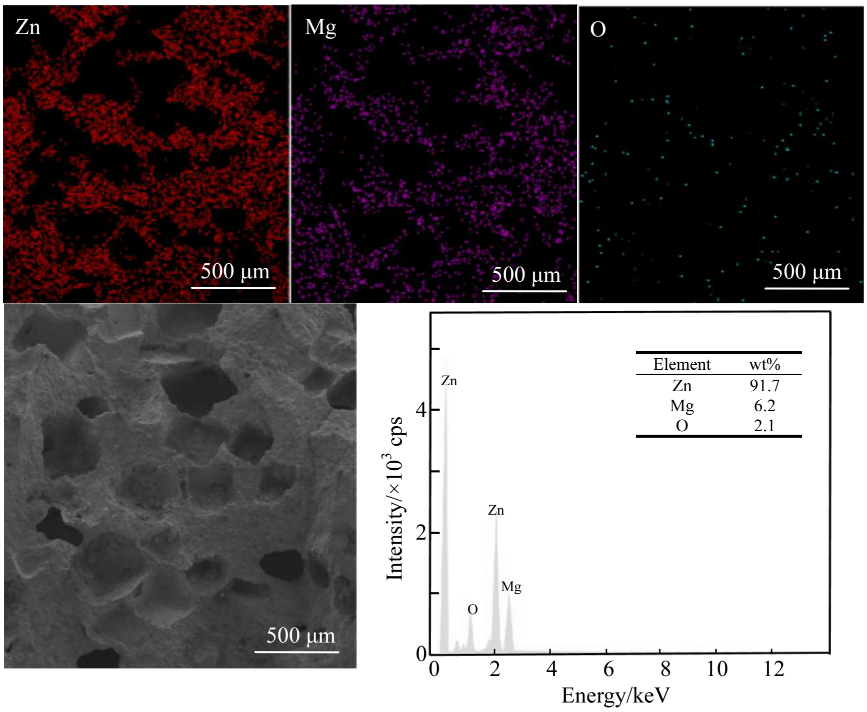

Fig.5 EDS analysis of inner pore structure of porous Zn-10Mg scaffold

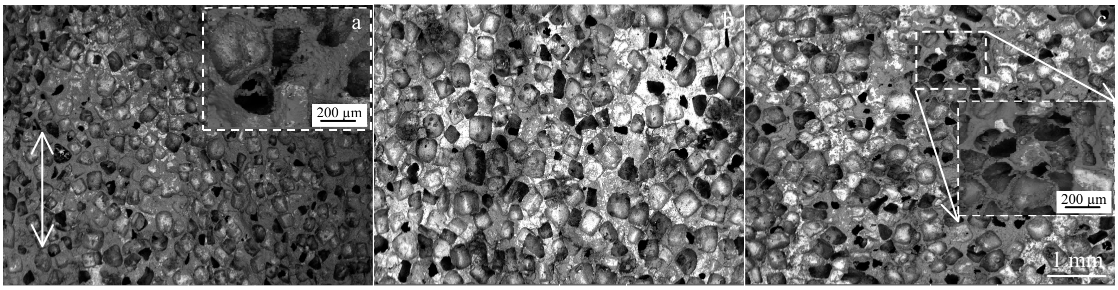

Fig.6 BSEM images of porous Zn-Mg scaffolds with different Mg mass contents (axial cross-section, the white arrows indicate pressure direction of SPS: (a) porous Zn-5Mg, (b) porous Zn-10Mg, and (c) porous Zn-15Mg

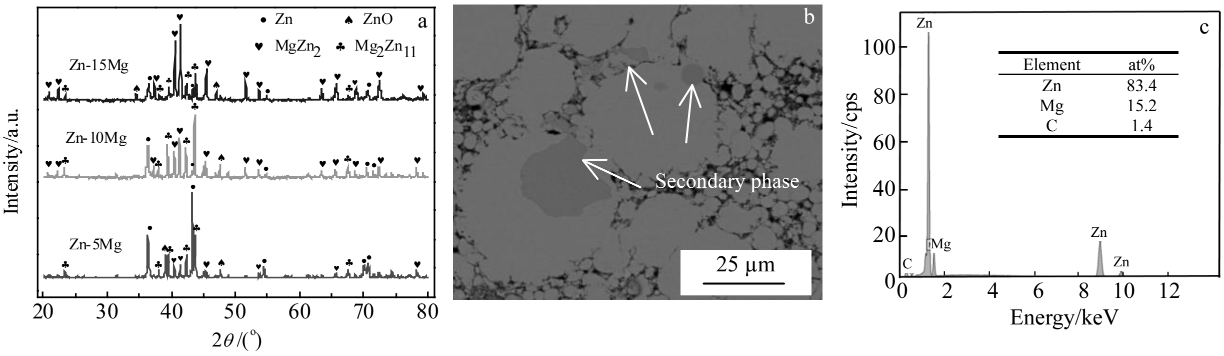

Element	at%
Zn	83.4
Mg	15.2
C	1.4

Fig.7 XRD patterns of sintered porous Zn-Mg alloy scaffolds (a), BSEM image of porous Zn-5Mg (b) and the EDS results of the arrowed point (c)

analysis of the secondary phase. The atom ratio between Zn and Mg element is nearly 5.5, indicating that the secondary phase can be confirmed as Mg_2Zn_{11} phase.

Furthermore, during the SPS process, with the help of spark discharge and pressure, the momentarily generated Joule heating between powder particles[18,19], could accelerate the alloying of Zn and Mg. It could be confirmed by the XRD patterns that with the increase of Mg content the peak of Zn decreases and the peaks of secondary (Mg_2Zn_{11}, $MgZn_2$) become stronger obviously.

2.3 Evaluation of mechanical properties

The mechanical properties of porous Zn-Mg binary alloy scaffolds are shown in Table 1. Because the prepared scaffolds would like to be mainly used for cancellous bone repair, excessive elastic modulus will induce stress shielding effects, which is not conducive to bone tissue healing. According to Ref. [3, 20], the yield compressive strength (YCS), Young's elastic modulus (E_c) and ultimate flexural strength (UFS) of human nature cancellous bone are 1.8~150 MPa, 0.1~20 GPa and 2~180 MPa, respectively. The elastic modulus and yield strength of porous Zn-Mg alloy scaffolds, which range from 1.5~7.6 GPa and 39~101 MPa, respectively, all can match the required range for lower load-bearing bone tissue application.

Compared with the porous Zn-based alloy scaffolds prepared by APIM[6,10,11], with the help of spark discharge and pressure during SPS, the pore wall of SPS sintered scaffolds is denser than that of the other method (Fig.6b and Fig.10). Hence, the porous Zn-Mg alloy scaffolds fabricated by SPS have higher mechanical properties. Besides, it could be found from these results that the mechanical properties of porous Zn-10Mg alloy scaffold were higher than those of the other two scaffolds. Generally, the mechanical properties of porous metal were determined by porosity and pore size[1,11-14]. However, in this work, the mechanical properties of porous Zn-Mg alloy scaffolds are not only a function of porosity and pore size, but also a function of Mg content. On the positive hand, Mg plays a role of alloying element for strengthening the mechanical properties by solid solution and precipitating the secondary phase ($MgZn_2$ and Mg_2Zn_{11}). On the negative hand, the addition of Mg also changes the porosity and pore size by dealloying during removing space holder process. As described by the classical Gibson-Ashby model [21], the elastic modulus and plateau strength have an inverse proportional exponential relationship between porosity, and the equations is shown as follows. Therefore, under the positive and negative effects of Mg, porous Zn-10Mg scaffold has excellent mechanical properties among porous Zn-Mg alloy scaffolds with three different mass content of Mg.

$$E/E_s = C_1(\rho/\rho_s)^{n_1} \tag{6}$$

$$\sigma_p/\sigma_y = C_2(\rho/\rho_s)^{n_2} \tag{7}$$

Where E is the elastic modulus of the porous scaffold, E_s is the elastic modulus of the solid bulk material, (ρ/ρ_s) is the relative density of porous scaffold, σ_p is the plateau strength of porous scaffold, σ_y is the yield strength of solid bulk material and C_1, C_2, n_1 and n_2 are constants depending on the pore structure.

2.4 Fracture mechanisms of the porous scaffolds

The compressive stress-strain curves of the studied materials are shown in Fig.8. Despite the different porosities and mass content of Mg, the compressive strength of the porous scaffolds exhibited a similar increasing tendency with the increase of strain. The compressive curves suggest that the

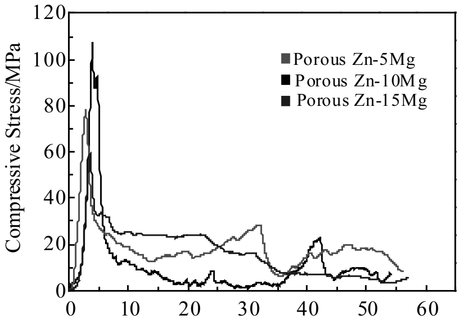

Fig.8 Compressive stress-strain curves of porous Zn-Mg alloy scaffolds sintered at 625 K

porous Zn-Mg alloy scaffolds are typical elastic-brittle metallic foam [14,19]. Because of the precipitation strengthening effect of secondary phase Mg_2Zn_{11} and $MgZn_2$ causing the plasticity worse, at the beginning, there was a short line-elastic deformation stage of less than 10% strain. Then a long stage with a little reduction or plateau of stress to large strain became more evident with the increase of porosity, about 20% strain for porous Zn-15Mg scaffold with 54.3% porosity. Actually, a temporary stress concentration occurred in the inner pore structure, pore structure broke, and then the stress was released. It means the pore structure was destroyed layer by layer. With the strain of porous Zn-5Mg scaffold increasing from 25% to 32% and strain of porous Zn-10Mg scaffold increasing from 35% to 42%, the stress all increased rapidly. This is a typical densification stage (Fig.9).

Fig.10 shows the flexural fracture surface of porous Zn-10Mg scaffold after three-point bending test. The flexural fracture surface is smooth without large deformation of pore structure, which suggests that the fracture mechanism of bending is more like brittle fracture. The flexural fracture process of the porous Zn-Mg scaffolds can be divided into two stages. At the beginning, the surface of porous area was subjected to external loading. When the stress reached the limit of deformation strength of pore wall materials (ultimate compressive strength), the micro-cracks were initiated and transmitted on the edge of weak pore wall and then form the original cracks. Then with external loading going on, the deformation around the original cracks in internal connected pore structure broke, and new micro-cracks initiated around the macro-cracks. Finally, the crack went across the entire section, and macroscopic fracture occurred in the porous sample. It could be seen clearly from Fig. 10b and 10c that the macro-crack extends along the weak pore wall and micro-cracks initiate around the macro-crack, which is in agreement with the above idea.

Table 1 Porosity, average pore size and mechanical properties of porous Zn-*x*Mg alloy scaffolds

Samples	Porosity/vol%	Pore size/μm	YCS/MPa	E_c/GPa	UFS/MPa	E_f/GPa
Porous Zn-5Mg	40.3	289	81	2.2	53	3.4
Porous Zn-10Mg	45.9	338	101	4.3	71	7.6
Porous Zn-15Mg	54.3	384	54	1.5	39	5.3
Porous Zn-3Cu (APIM) [10]	68	400-450	11.42	0.95	-	-
Porous Zn-3.5Ag (APIM) [11]	59	329	13.7	-	-	-
Nature cancellous bone [3,20]	-	-	1.8~150	0.1~20	2~180	0.1~20

Note: YCS-yield compressive strength, E_c- elastic modulus of compression, UFS- ultimate flexural strength, E_f- elastic modulus of flexure

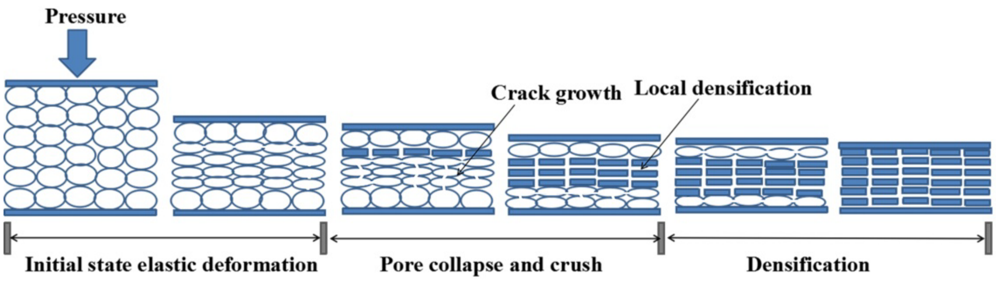

Fig.9 Schematic diagram of typical compressive deformation mechanism of metallic porous scaffold

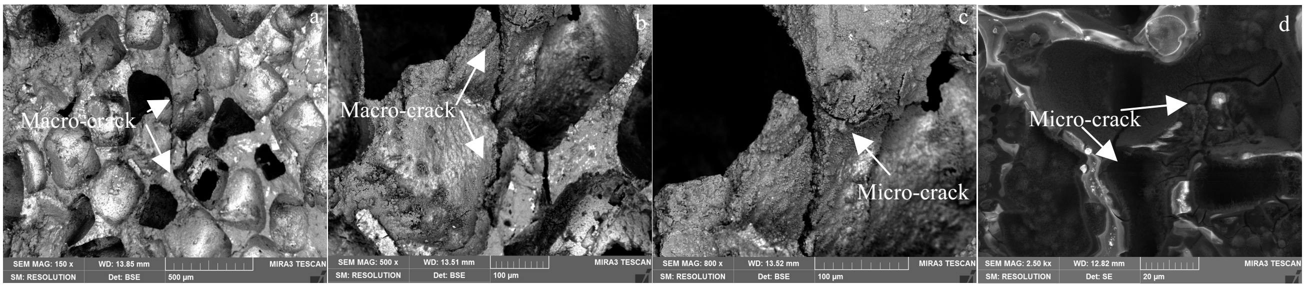

Fig.10 BSEM images of flexural fracture surface (porous Zn-10Mg with 45.9% porosity, white arrows indicating the cracks): (a, b) morphologies of macro-cracks and pore structure, (c, d) magnified images of the micro-cracks formed after testing on the pore walls

3 Conclusions

1) With the addition of Mg increasing from 5% to 15%, the open pore size of scaffolds increases from 289 μm to 384 μm, and porosity increases from 40.3% to 54.3%, due to dealloying effect of remained pure Mg when removing NaCl particles.

2) With the help of spark discharge and pressure from spark plasma sintering, a sufficient metallurgical reaction between zinc and magnesium produces a large amount of secondary phase ($MgZn_2$, Mg_2Zn_{11}).

3) The porous Zn-Mg alloy scaffold is a typical brittle metal foam. The yield stress and *E* modules value of the porous Zn-*x*Mg scaffolds all match the required range for lower load-bearing bone application.

References

1 Liao Y L, Qiu G B , Yang Y *et al*. *Rare Metal Materials and Engineering*[J], 2016, 45(10): 2498 (in Chinese)

2 Čapek J, Vojtěch D. *Materials Science and Engineering C*[J], 2013, 33(1): 564

3 Yan Y, Kang Y J, Li D *et al*. *Journal of Materials Engineering and Performance*[J], 2018, 27: 970

4 Bowen P K, Drelich J, Goldman J. *Advanced Materials*[J], 2013, 25(18): 2577

5 Čapek J, Jablonska E, Lipov J *et al*. *Materials Chemistry and Physics*[J], 2013, 203: 249

6 Zhao L C, Zhang Z, Song Y T *et al*. *Materials and Design* [J], 2016, 108 : 136

7 Sadighikia S, Abdolhosseinzadeh S, Asgharzadeh H. *Powder Metallurgy*[J], 2015, 58(1): 61

8 Li H F, Xie X H, Zheng Y F *et al*. *Scientific Reports*[J], 2015, 5: 10 719

9 Vojtěch D, Kubásek J, Šerák J *et al*. *Acta Biomaterialia*[J], 2011, 7(9): 3515

10 Hou Y, Jia G Z, Yue R *et al*. *Materials Characterization*[J], 2018, 137: 162

11 Xie Y, Zhao L C, Zhang Z *et al*. *Materials Chemistry and Physics*[J], 2018, 219: 433

12 Xie Fangxia, He Xueming, Yu Jinghu *et al*. *Rare Metal Materials and Engineering*[J], 2016, 45(6): 1477 (in Chinese)

13 Deng Zhenbo, Zhou Changchun, Fan Yujiang *et al*. *Rare Metal Materials and Engineering*[J], 2016, 45(9): 2287 (in Chinese)

14 Wang Q B, Li G Z, Tang H P *et al*. *Rare Metal Materials and Engineering*[J], 2017, 46(9): 284 (in Chinese)

15 Hao G L, Wang H, Li X Y *et al*. *Rare Metal Materials and Engineering*[J], 2016, 46(9): 2379 (in Chinese)

16 Jamesh M I, Wu G, Zhao Y *et al*. *Corrosion Science*[J], 2015, 91: 160

17 Okamoto H. *Journal of Phase Equilibria and Diffusion*[J], 2013, 34: 251

18 Lee J, Wang J H, Lee D *et al*. *Journal of Alloys and Compound*[J], 2014, 617: 505

19 Zhang L, He Z Y, Zhang Y Q *et al*. *Materials and Design*[J], 2016, 101: 170

20 Rezwan K, Chen Q Z, Blaker J J *et al*. *Biomaterials*[J], 2006, 27: 3413

21 Gibson L J, Ashby M F. *Cellular Solids: Structure and Properties*[M]. Cambridge: Cambridge University Press, 1997: 183

放电等离子烧结制备医用多孔锌镁合金的孔隙特征和力学行为

崔泽琴 [1,2,3]，李伟健 [1,2,3]，马丽莉 [1]，杨蕊鸿 [1]，宫殿清 [1,2,3]

(1. 太原理工大学，山西 太原 030024)
(2. 先进镁基材料山西省重点实验室，山西 太原 030024)
(3. 新材料界面科学与工程教育部重点实验室，山西 太原 030024）

摘　要：采用放电等离子烧结技术制备多孔Zn-Mg合金，探讨了Mg含量对多孔合金孔隙特征和力学性能的影响，并分析了多孔Zn-Mg合金的断裂失效机制。结果表明，在造孔剂 (NaCl) 体积分数固定前提下当Mg含量从5%增加至15%（质量分数），由于在去除造孔剂的过程中去合金化作用，孔隙率从40.3%提升至54.3%，表面开孔直径从289 μm增加到384 μm。力学测试结果表明，多孔Zn-Mg合金为一种弹脆性多孔材料；3种组分中多孔Zn-10Mg合金力学性能最好，其强度与弹性模量均能满足作为承受低载荷松质骨的需求。

关键词：多孔锌合金；放电等离子烧结；孔隙结构；力学性能

作者简介：崔泽琴，女，1977 年生，博士，副教授，太原理工大学材料科学与工程学院，山西 太原 030024，E-mail: cuizeqin@tyut.edu.cn